# Longitudinal in-vivo Volumetry Study for Porcine Liver Regeneration from CT Data

Jiayin Zhou, *IEEE Member*, Weimin Huang, *IEEE Member*, Stephen K.Y. Chang, Wei Xiong, *IEEE Member*, Thiha Oo, and Wenyu Chen

***Abstract*—The use of hepatic-like cloned cord lining epithelial cells (CLEC) to enhance liver regeneration has been proposed, but has not been properly investigated in a large animal study. The paper presents a system developed for the longitudinal in-vivo volumetry study on porcine liver regeneration from computed tomography (CT) data. In this system, a rough 3D liver volume is firstly automatically segmented by a 3D mesh deformation-based method. Then a refinement step to eliminate the segmentation error is carried out by a 3D post-editing tool, followed by mesh-volume conversion and volume calculation. This system was applied in a pilot study, which was composed of 4/4 pigs in the Experimental/Control Groups, to measure liver volumes over pre- to post-operative time course. Experimental results suggest that (1) the developed system can perform CT-based porcine liver volumetry efficiently, and (2) the infusion of CLEC to liver remnant may potentially enhance the liver regeneration.**

## I. Introduction

Liver cancer, a serious threat to human health due to its high mortality, ranks as the sixth most frequent malignancy in the world [1][2]. Compared to other treatment options such as thermal ablation, embolization and chemotherapy, partial liver resection (hepatectomy) offers the best long-term prognosis if the tumor is resectable [3]. The overall selection criteria on lesion number, size and location for hepatectomy are strict, although downstaging approaches may be performed to reduce the tumor size for the subsequent resection. As an aggressive liver resection can result in the remnant liver with insufficient liver function, the extent of hepatectomy is balanced against risk of acute post-operative liver failure. This restriction applies in liver transplant as well. Patients with end-stage chronic liver diseases as well as severe acute liver decompensation can all benefit from liver transplant, especially the living donor liver transplant (LDLT). However a scarcity of liver donors and a need for lifelong immunosuppressants means the selection for donor is even stricter, hence patients may die while waiting for a transplant. To address this problem, many attempts have been made to enhance the regeneration of the damaged liver.

The capacity of the liver to regenerate and maintain a constant size despite injury is unique, but the exact mechanisms are not completely clear. Cell transplantation, especially the infusion of hepatic-like cloned cord lining epithelial cells (CLEC), has been proposed as a novel alternative treatment of liver diseases [4][5]. CLECs are prepared from umbillcal cord lining which is easily obtainable, hence CLEC are immunologically naive and represent few ethical dilemma, compared to using embryonic stem cells. The use of CLEC to enhance liver regeneration has not been properly investigated in a large animal study. In an ongoing exploratory project conducted in the National University Hospital of Singapore, the efficacy of hepatic-like cloned CLEC in post-hepatectomy liver regeneration is being investigated, by using a porcine liver resection model.

To understand the change of liver volume over the time course, robust and reliable porcine liver volumetry plays an important role. Literature search shows that in-vivo computed tomography (CT)-based liver volumetry acquires accurate data as confirmed by ex-vivo water displacement-based volumetry, regardless the difference caused by blood perfusion [6]. Compared to interactive and manual volumetry, automated image segmentation and volumetry is substantially more efficient [7]. There are quite a few algorithms developed for automated 2D-/3D-based liver segmentation on human, however no such study on porcine liver segmentation has been reported. In this paper, we present (1) a mesh deformation method to segment and quantify the porcine liver 3D volume from CT data for the longitudinal in-vivo study of liver regeneration, and (2) the pilot data to compare post-operative liver regeneration with and without CLEC infusion.

## II. Method

### A. Porcine Liver Anatomy and CT Imaging

Figure 1 shows a dissected porcine liver. By external deep interlobular fissures, a porcine liver can be divided into 4 big lobes (right lateral, right median, left median and left later lobes) and 1 small lobe (caudate lobe which adjoins the right lateral lobe on the visceral surface). The lobular nature of the porcine liver makes it easier to be divided anatomically into 2 approximate hemi-livers than the human liver. Internally, a porcine liver can be divided into 8 segments by the vascular structure, similar to the human liver [8]. Contrast-enhanced CT images of porcine liver in portal venous (PV) phase are shown in Fig. 2. The appearance and shape of porcine liver in CT images is generally similar to those of human liver, but some considerable differences exist, including the wider span of the left lateral lobe to the left abdominal cavity, the thinner right lobes, the sharper shape changes occur at the lobe periphery and interlobular fissures, etc.

This work was supported by (1) a research grant (JCOAG03-FG05-2009) from the Joint Council Office, Agency for Science, Technology and Research (A*STAR), Singapore and (2) a research grant (NMRC/EDG/1059/2012) from the National Medical Research Council, Ministry of Health, Singapore.

J. Zhou, W. Huang, W. Xiong, T. Oo and W. Chen are with the Institute for Infocomm Research, A*STAR, Singapore 138632 (corresponding author: J. Zhou; phone: +65 6408-2497; e-mail: jzhou@i2r.a-star.edu.sg).

S.K.Y. Chang is with the Department of Surgery, National University Hospital, Singapore 119074.

978-1-4244-7929-0/14/$26.00 ©2014 IEEE

Figure 1. A porcine liver in visceral (left) and diaphragmatic (right) surfaces

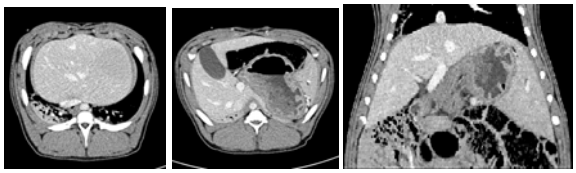

Figure 2. PV-phase CT images: Left, an axial image in an upper section; Middle, an axial image in a lower section; Right, a coronal image.

### *B. Automated CT Liver Image Segmentation*

There are a number of 2D-/3D-based methods reported for human liver segmentation from CT scan. Some typical methods include the statistical shape model with optimal surface detection [9], graph cut [10], 2D approximate contour model [11], hierarchical learning-based approach [12], etc. For our application, the shapes of the porcine liver represented in pre- and post-operative scans are quite diverse, hence it is difficult to construct the statistical shape model which is applicable to deform and fit to the actual liver object. This diversity occurs in image texture pattern as well. In addition, one animal subject can have several longitudinal scans, which may make the database huge especially for a large clinical trial. Therefore a 3D-based fast segmentation algorithm with less shape prior/constraint is the preference.

In this study, a mesh deformation model has been developed to segment the 3D liver volume from CT data by iteratively deforming a 3D mesh model and registering it to the extracted image features. Each step of the method is explained as follows:

(1) Definition of 3D spherical quadrilateral mesh: Firstly, a 3D quadrilateral mesh $M$ on a cube whose sides are aligned with $x$-, $y$- and $z$- axis is defined. The mesh is defined by 3 groups of closed contours $G_{xy}$, $G_{xz}$ and $G_{yz}$, which are parallel to the $xy$-, $yz$- or $zx$- plane respectively. The contours in each group are orthogonal to those in the other groups. Each vertex in $M$ is an intersection of two contours, each from a different group and with exactly 4 connected neighboring vertices. The cubical quadrilateral mesh is then mapped to a spherical quadrilateral mesh by projecting its mesh vertices onto a concentric spherical surface along the radius directions, as shown in Fig. 3.

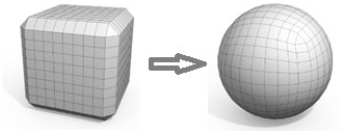

Figure 3. The mapping of a cubical quadrilateral mesh to a spherical quadrilateral mesh

(2) Extraction of image features: The segmentation algorithm can tackle with various image features including intensity, gradient, edge, texture, etc. In this study, the distribution of voxel densities was adopted, as the liver volume may have heterogeneous voxel densities and some object boundaries are indistinct. The density distribution of the liver is modeled as a mixture of Gaussians

$$g(x) = \sum_i a_i f_i(x), \qquad (1)$$

where $x$ is the voxel density, $a_i$ are coefficients and $\sum_i a_i = 1$, and $f_i(x)$ are Gaussian distributions with parameters $(\mu_i, \sigma_i)$. The number of Gaussians is determined by the input images. Parameters $a_i$, $\mu_i$ and $\sigma_i$ can be estimated by expectation maximization (EM). To smooth out the noise, the input image is pre-processed by an anisotropic diffusion filter.

(3) Deformation: Unlike implicit model-based deformable methods which represent a 3D surface as an implicit function discretized into voxels, explicit model-based deformable methods represent a 3D surface as a mesh. It can significantly reduce the space complexity, but deformation is accomplished by the displacement of the mesh vertices, which may cause self-intersection of the mesh [13]. Flipping self-intersection occurs locally if the displacement vectors of neighboring mesh vertices cross in space. As a result, the directions of some surface normals flip after deformation. Non-flipping self-intersection occurs globally without flipping the surface normals but causes penetration of different parts of the mesh. In this study, within each iteration of mesh deformation, possible correspondence between mesh vertices and image features over long distances is searched, and then the detected correspondence is refined before the actual deformation to avoid flippings. In implementation, the point correspondences of flipping vertices were discarded, hence only non-flipping vertices have point correspondences after repeating this process for every closed contour. As a result, deforming the mesh according to these correspondences does not result in flipping. To avoid non-flipping self-intersections, displacement vectors of non-flipping vertices were propagated to neighboring solitary vertices, turning them into non-flipping vertices by iterative local averaging of displacement vectors. This process is analogous to the diffusion of gradient vectors. In the meanwhile, it can also smooth over the variation of displacement vectors among neighboring non-flipping vertices, thus improving noise tolerance.

### *C. Implementation, Post-Editing and Volume Calculation*

This algorithm was implemented by C++ with ITK/VTK toolkits and integrated into a QT-built interface. Before the deformation starts, the user needs to click a point inside the liver and by using this point as the centroid, a small 3D sphere which is totally inside the liver is generated as the initial spherical mesh. Voxels inside the sphere are used to build a GMM of the density probability distribution of the target liver (foreground). Voxels with low probability are regarded as background featured voxels. Transitions from consecutive foreground voxels to consecutive non-liver voxels along searching directions suggest the presence of boundary points of the target liver. The whole segmentation process can be completed within 2 minutes, in a PC workstation with Intel Core i7 2.8 GHz CPU and 8G memory. Figure 4 shows the

evolution of the mesh deformation at iterative Cycles 0, 10, 25 and 60, for a pre-operative porcine live. It is observed that the segmentation is almost completed at Cycle 60.

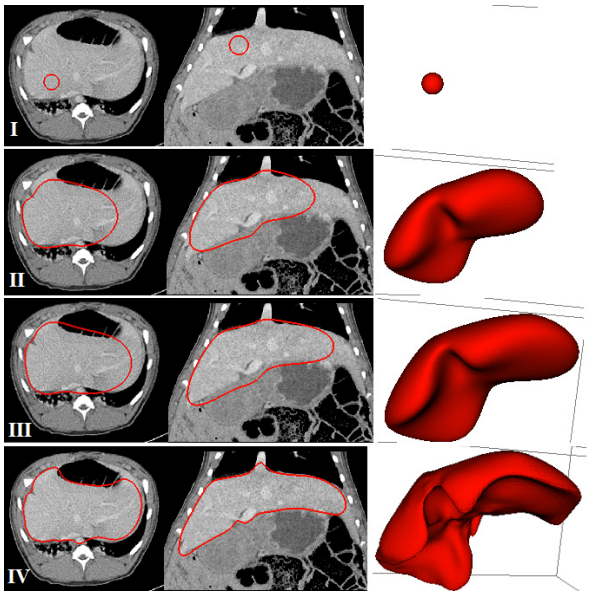


Figure 4. The evolution of mesh deformation at different iterative cycles for porcine liver segmentation. Row I: the initial spherical mesh (Cycle 0), Row II: at Cycle 10, Row III: at Cycle 25, and Row IV: at Cycle 60.

After the automated 3D segmentation, the majority of the porcine liver will be well segmented, with some common over- and under-segmentation errors described below: (1) the over-segmentation occurs at the interface of the liver and the pulmonary tissue in the right inferior lateral due to the close tissue densities, as shown in Fig. 5; (2) the inclusion of a trunk of inferior vena cava (IVC) in the lower section due to the similar tissue densities; (3) the over-/under-segmentation of the regenerated liver parenchyma near the resection plane, due to the density heterogeneity of the regenerated liver parenchyma, etc. Hence a 3D mesh editing tool, whose functions include singular structure removal, object(s) connecting/separating, local volume expending/erosion, re-contouring, etc., has been developed for the post-editing of the segmented porcine liver. This tool has also been implemented in the same QT interface and by using this tool, the segmented object can be refined within 5 minutes. After refinement, the mesh model will be converted into the volumetric file for volume calculation.

## III. Experiment

The developed segmentation-editing tool was evaluated on 20 PV-phase CT scans of human liver. By calculating the Jaccard Index based on volex matching, segmentation results were benchmarked with ground truths which were labeled by the clinician. An averaged Jaccard Index of 0.93±0.04 (min. 0.88, max. 0.97) was achieved.

The porcine experiment protocol was approved by the Institutional Review Board, National University of Singapore (NUS). A 50% (approximately) liver resection by removing left median and left lateral lobes was performed on eight pigs (6-month old) to create the liver regeneration model. A portal vein catheter was implanted for each pig during surgery. These pigs were randomly assigned into two groups:

**Experimental Group**: 4 pigs received the tissue fleece with the hepatic like cloned CLEC placed on the surface of the resected liver immediately after surgery and daily injection of cells for 7 days via the portal-catheter.

**Control Group**: 4 pigs received the tissue fleece without cells and no injection of cells after surgery.

All pigs were housed in the Comparative Medicine Centre of NUS, with standardized post-operative housing and nutrition regimes. Standard four-phase contrast-enhanced CT scans on the abdomen were performed for all pigs at 2 days before the operation (PreO), post-operative Day 0 (POD0), Day 7 (POD7) and Day 14 (POD14), respectively, by a 128-detector CT system (SOMATOM Definition, Siemens). For each scan, PV-phase images were exported for image segmentation and volumetry, with the following parameters: slice thickness of 1.5 mm, matrix of 512×512 pixels and inplane resolution of 0.69–0.75 mm.

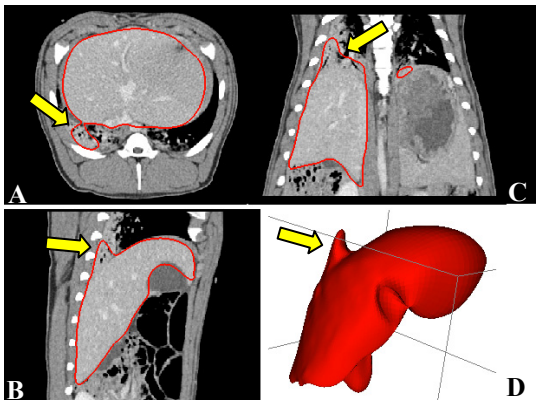


Figure 5. An over-segmentation error: a small portion of the neighboring pulmonary tissue in the right inferior lateral of the liver was included. A, B and C: 2D images from axial, sagittal and coronal planes; D: the 3D view.

## IV. Results

Totally 32 (8x4) CT data sets were processed, including the 3D mesh deformation-based segmentation, 3D post-editing and volume calculation. The liver volumes of the eight pigs on PreO, POD0, POD7 and POD14 are tabulated in Table 1. The changes of averaged percentage of liver volume to the baseline (volume on PreO) over the time course are shown in Figure 6. Liver regeneration in both Experimental

TABLE I. Porcine Liver Volume Changes Over Time Course

| Liver volume (mL) | PreO | POD0 | POD7 | POD14 |
|---|---|---|---|---|
| Expt. Group | | | | |
| #1 | 1227 | 523 | 941 | 1109 |
| #2 | 1223 | 490 | 974 | 1117 |
| #3 | 1045 | 498 | 876 | 904 |
| #4 | 1273 | 657 | 1084 | 1135 |
| Control Group | | | | |
| #1 | 1460 | 801 | 1166 | 1267 |
| #2 | 1156 | 496 | 701 | 743 |
| #3 | 1252 | 561 | 689 | 890 |
| #4 | 1094 | 515 | 728 | 823 |

and Control Groups was fast. For Control Group, the liver volume restored to 67% and 75% of the original volume on POD7 and POD14, respectively. For Experimental Group, the liver volume restored to 81% and 89% of the original volume on POD7 and POD14, respectively. This may suggest the potential usefulness of hepatic like cloned CLEC in enhancing liver regeneration. Moreover, the pilot data support the feasibility of a subsequent large-scale animal trial.

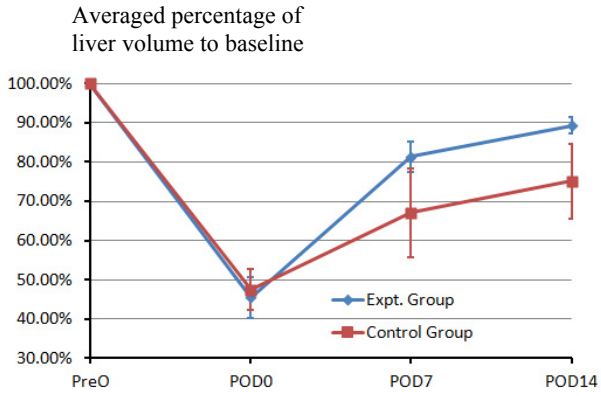


Figure 6. Changes of the averaged percentage of liver volume to the baseline over the time course for Experimental Group and Control Group

The changes of one porcine liver morphology in 2D CT images and 3D view from PreD to POD14 are displayed in Fig. 7. It can be observed that after the resection of left median and left lateral lobes, the majority of the regeneration is the thickening of right lateral and right median lobes, with slight regrowth along the resection plane surface to the left lateral of abdominal cavity.

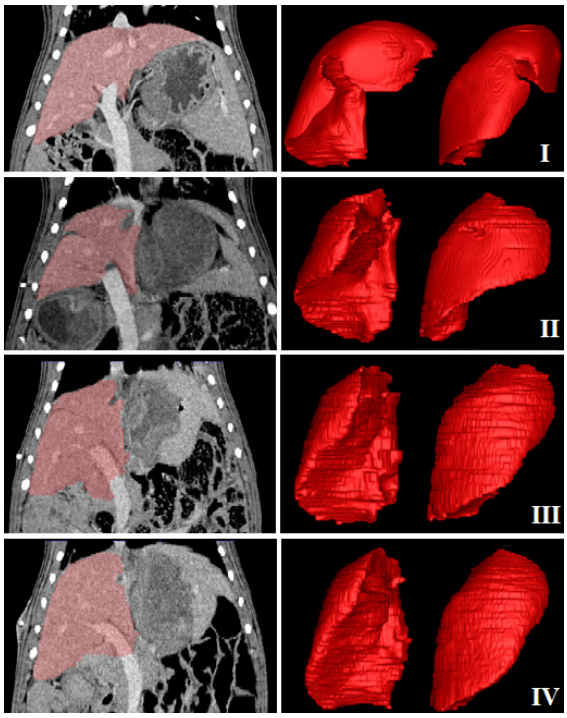


Figure 7. Changes of liver morphology in 2D CT images and 3D view on PreO, POD0, POD7 and POD14 (Row I to Row IV), respectively

## V. Conclusion

A porcine liver volumetry system using a 3D mesh deformation-based segmentation method and a post-editing tool has been developed. This system was applied in a longitudinal in-vivo assessment of liver regeneration in 8 porcine liver resection models. Pilot experimental results suggest that (1) the developed system can perform CT-based liver volumetry efficiently, and (2) the infusion of hepatic-like cloned CLEC to liver remnant may potentially enhance the liver regeneration. In addition, the system developed and the pilot data support the feasibility of a large-scale animal trial, to investigate the efficacy of CLEC in liver regeneration.

## Acknowledgment

Authors hereby thank the contribution from the veterinary and animal care team, School of Medicine, NUS.

## References

[1] A. Ananthakrishnan, V. Gogineni, and K. Saeian, Epidemiology of primary and secondary liver cancers, Semin. Intervent. Radiol., vol. 23, no. 1, pp. 47-63, Mar. 2006.

[2] F.X. Bosch, J. Ribes, M. Díaz, et al., Primary liver cancer: worldwide incidence and trends. Gastroenterology, vol. 127, no. 5 supp. 1, pp. S5-S16, Nov. 2004.

[3] L. Zhou, C. Liu, F.D. Meng, et al., Long-term prognosis in hepatocellular carcinoma patients after hepatectomy, Asian Pac. J. Cancer Prev., vol. 13, no. 2., pp. 483-486, 2012.

[4] A.A. Khan, M.V. Shaik, N. Parveen, et al., Human fetal liver-derived stem cell transplantation as supportive modality in the management of end-stage decompensated liver cirrhosis, Cell Transplant., vol. 19, no. 4, pp. 409-418, Apr. 2010.

[5] Y. Zhou, S.U. Gan, G. Lin, et al., Characterization of human umbilical cord lining-derived epithelial cells and transplantation potential, Cell Transplant., vol. 20, no. 11-12, pp. 1827-1841, Nov. 2011.

[6] S.M. Niehues, J.K. Unger, M. Malinowski, et al., Liver volume measurement: reason of the difference between in vivo CT-volumetry and intraoperative ex vivo determination and how to cope it, Eur. J. Med. Res., vol. 15, no. 8, pp. 345¨C350, Aug. 2010..

[7] K. Suzuki, M.L. Epstein, R. Kohlbrenner, et al., Quantitative radiology: automated CT liver volumetry compared with interactive volumetry and manual volumetry, AJR Am. J. Roentgenol., vol. 197, no. 4, pp. 706-712, Oct. 2011.

[8] F.G. Court, S.A. Wemyss-Holden, C.P. Morrison, et al., Segmental nature of the porcine liver and its potential as a model for experimental partial hepatectomy, Br. J. Surg., vol. 90, no. 4, pp. 440-444, Apr. 2003.

[9] X. Zhang X, J. Tian, K. Deng, et al., Automatic liver segmentation using a statistical shape model with optimal surface detection, IEEE Trans. Biomed. Eng., vol. 57, no. 10, pp. 2622-2626, Oct. 2010.

[10] R. Beichel, A. Bornik, C. Bauer, et al., Liver segmentation in contrast enhanced CT data using graph cuts and interactive 3D segmentation refinement methods. Med. Phys., vol. 39, no. 3, pp. 1361-1373, Mar. 2012.

[11] M. Ciecholewski, Automatic liver segmentation from 2D CT images using an approximate contour model, J. Sign. Process. Syst., vol. 74, no. 2, pp. 151-174, Feb. 2014.

[12] H. Liang, S.K. Zhou, Y. Zheng, et al., Hierarchical, learning-based automatic liver segmentation, in Proc. Computer Vision and Pattern Recognition (CVPR), 23-28 June 2008.

[13] J.E. Gain, and N.A. Dodgson, Preventing self-intersection under free-form deformation, IEEE Trans. Vis. Comput. Graph., vol. 7, no. 4, pp. 289-298, Oct.-Dec. 2001.